EPJ Web of Conferences **147**, 04004 (2017)
DOI: 10.1051/epjconf/201714704004
EC-19

Remote-Steering Antennas for 140 GHz Electron Cyclotron Heating of the Stellarator W7-X

C. Lechte[1,a], W. Kasparek[1], B. Plaum[1], A. Zeitler[1], V. Erckmann[2], H. Laqua[2], N. Schneider[2], M. Weissgerber[2], A. Bechtold[3], M. Busch[4], and B. Szepaniak[4]

[1] *Institute of Interfacial Process Engineering and Plasma Technology IGVP, University of Stuttgart, Germany*
[2] *Max-Planck-Institut fuer Plasmaphysik, Boltzmannstr. 2, 85748 Garching, Germany*
[3] *NTG Neue Technologie GmbH & Co KG, 63571 Gelnhausen, Germany*
[4] *Galvano-T electroplating-electroforming GmbH, 51570 Windeck-Rosbach, Germany*

Abstract. For electron cyclotron resonance heating of the stellarator W7-X at IPP Greifswald, a 140 GHz/10 MW cw millimeter wave system has been built. Two out of 12 launchers will employ a remote-steering design. This paper describes the overall design of the two launchers, and design issues like input coupling structures, manufacturing of corrugated waveguides, optimization of the steering range, integration of vacuum windows, mitrebends and vacuum valves into the launchers, as well as low power tests of the finished waveguides.

1 Introduction

The ECRH system at the stellarator Wendelstein 7-X (W7-X) has 10 MW of continuous power at 140 GHz [1]. The beams from the 10 gyrotrons are transmitted via 2 quasi-optical multi-beam transmission lines. In addition to the conventional equatorial launchers with front steering mirrors, launchers in the N ports allow quasi-high field side injection into the plasma. However, since the N ports are much smaller, it was not feasible to use front steering mirrors.

The remote steering principle uses corrugated square waveguides which image a tilted beam from the input to the output side. At the output, no movable parts are necessary and the waveguide can end flush with the vessel wall. This makes the remote steering solution very compact and suitable for use in a fusion power plant.

In W7-X, 2 beams can be rerouted from the front steering launchers to the remote steering launchers (RSL1 and RSL5, see Fig. 1.) The RSLs are water cooled for cw operation and they incorporate vacuum elements (diamond window and plate valve) as well as a mitre bend.

The design and manufacture of the RSLs were done within the framework of the FORMIK[3] project with financial support from the German Federal Ministry for Education and Research. The main components were fabricated by the industrial partners NTG and Galvano-T.

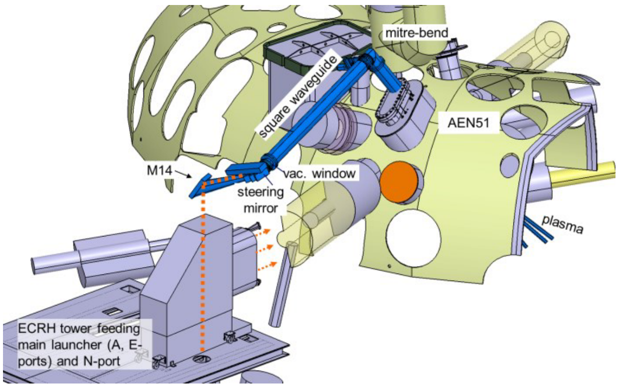

Figure 1. Concept of the remote steering launcher RSL5 for W7-X

2 The remote steering principle

The remote steering method using corrugated square waveguides employs the Talbot effect [2] to image the input pattern at the output side. This effect takes place if the length L of the waveguide with width a is as in Eq. (1). If the input pattern represents a Gaussian beam with tilt or steering angle Φ, then the output pattern represents the same beam but with steering angle –Φ. This is shown in Fig. 2. The beam pattern is made up of several waveguide modes which propagate with different phase speeds. At the end of the waveguide, the phase differences are an integral number of π again and the pattern in recreated.

Since the imaging effect depends on a paraxial approximation, it breaks down for large (>12˚) angles (Fig. 2, bottom plot.) This manifests as an incorrect

[a] Corresponding author: carsten.lechte@igvp.uni-stuttgart.de

DOI: 10.1051/epjconf/201714704004

length of the waveguide. A formula that corrects for the steering angle Φ is given in Eq. (2).

$$L = 4\, a^2 / \lambda \qquad (1)$$

$$L_{corr} = L / (1 + 0.5 \sin^2 \Phi) \qquad (2)$$

As a consequence, for larger steering angles, the RSL needs to be slightly shorter [3]. For a steering angle of 22.4˚, the waveguide is long enough for the beam to complete another internal reflection and produce an output beam that goes into the opposite direction (revival).

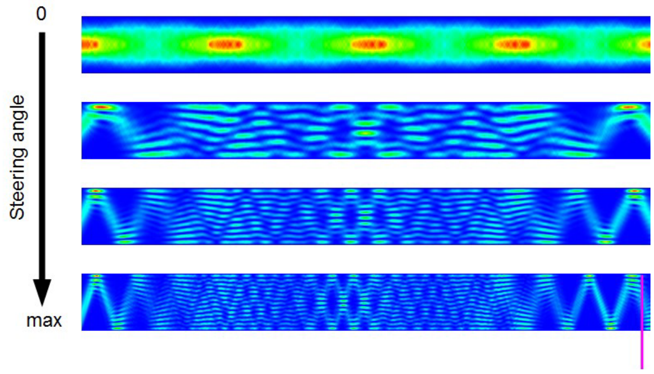

Figure 2. Field pattern in a corrugated rectangular waveguide for tilted input beams. For large angles, the beam shifts so far off-centre, that it hits the waveguide wall.

3 Design for W7-X

In order to fit into the W7-X ECRH system, the RSL waveguides needed to incorporate a mitrebend near the middle of its length. Its corrugation was carefully optimised to form a smooth transition between the 2 directions.

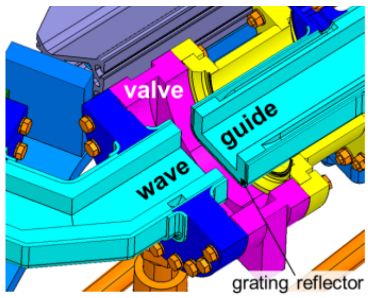

Figure 3. Incorporation of vacuum valve at the mitrebend.

The inside would be under vessel vacuum, with a diamond vacuum window at the input side. An additional vacuum valve was necessary in case of window failure. Since this leaves a 20 mm gap in the waveguide, it was located at half length, where the field at the waveguide walls is minimal and therefore stray radiation is minimised. A grating reflector keeps stray radiation away from the heat sensitive vacuum valve O rings.

Because of the large Brillouin angle of the beam inside the waveguide (see Fig. 2), ohmic losses are expected to be in the 1-2 % range when using copper material. Therefore, water cooling is mandatory to enable cw operation.

The width of the waveguides is approximately 50 mm and the length approximately 5 m.

4 Optimisation of the corrugation profile

To design a corrugation profile that meets high power cw specifications, extensive fullwave simulations were made [4]. For the hybrid modes in the waveguide to propagate correctly, a corrugation period of 0.8 mm and an effective depth of λ/4 is necessary. The profile must have a rounded shape to avoid arcing, but still must have a 180˚ phase difference between the TE and TM modes. Finally, to minimise ohmic losses, the grooves should be wider than the ridges. The waveguide was manufactured by electroforming, i.e. the negative form was machined in aluminium and the waveguide made from electroformed copper.

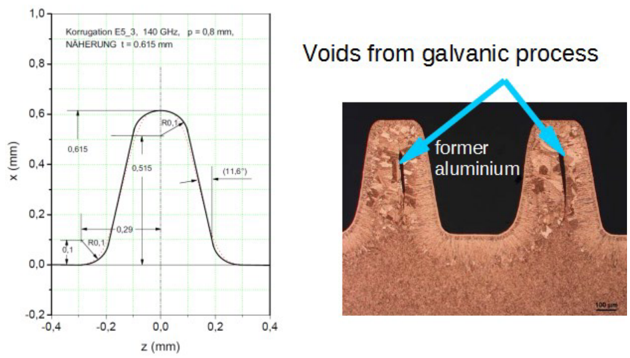

Figure 4. Corrugation profile (left) and cut of a test piece (right) after electroforming.

The chosen corrugation profile is shown in Fig. 4. Because of the manufacturing process and the cooling (heat conduction) requirements, the ridges could not be made very thin. Even so, voids have formed in the material of the ridges because of the complicated growth pattern of the electroformed copper inside the grooves of the aluminium mandrel. The voids were found to be unproblematic for the functioning to the waveguide.

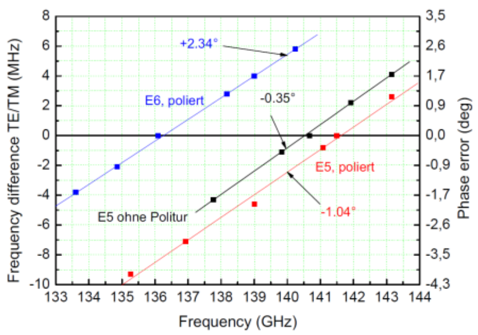

Figure 5. Measurement of the phase error between the 2 polarisations at various frequencies.

 DOI: 10.1051/epjconf/201714704004

5 Optimisation of the steering range

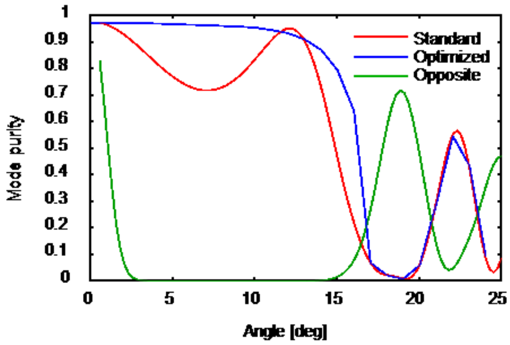

Figure 6. Mode purity of the output Gaussian beam for different steering angles with an optimum waveguide length for 12.7°.

The non-optimised usable steering angle range of 12° was unsatisfactory for the W7-X system. A variable mechanical length change according to the current steering angle is not feasible for a water-cooled, corrugated waveguide. Therefore, a virtual length adjustment was designed by way of an optimised input coupling. The increasing lateral displacement of the beam at large steering angles was counteracted by a lateral displacement at the input side, which is equivalent to shifting the intercept of the input beam with the waveguide axis into the waveguide, effectively shortening it to the ideal length given in Eq. (2).

In addition, the length of the waveguide was set to the ideal length for a steering angle of 12.7°. The resulting deterioration of the beam quality for lower angles (see red curve in Fig. 6) was again compensated by the optimised input coupling, which shifts the beam in the other direction, effectively lengthening the waveguide. The result can be seen in Fig. 6, blue curve, which shows a usable beam from 0° up to 16° steering angle. Finally, the revival of the beam in the opposite direction is shown in green.

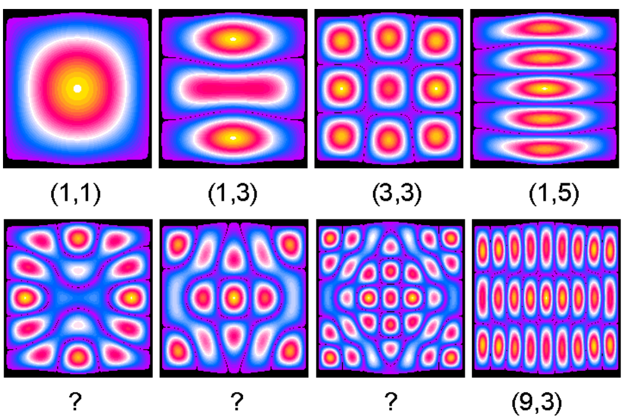

Figure 7. Perpendicular mode patterns in the deformed waveguide cross section for A=2 mm and q = 4.

A different approach to the improvement of the steering range was the modification of the dispersion relation inside the waveguide itself. This can be achieved by deformation of the cross section of the waveguide. The deformations were of the shape A $\cos(x)^q$ where A is the amplitude (up to a few percent of the waveguide width) and q is an integer between 2 and 5. The modes and propagation constants of the deformed waveguide were calculated with the IPF-FD3D [5] code.

Some resulting modified mode patterns are shown in Fig. 7. While some modes have clear correspondences to the undeformed modes, some patterns are not. Together with the modified propagation constants, the imaging properties of the deformed waveguide could be simulated with the PROFUSION code.

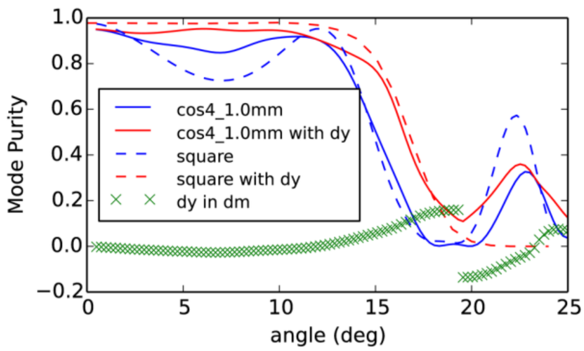

Figure 8. Mode purities of the deformed vs. the undeformed waveguides. dy is the lateral displacement from the optimised input coupling.

As can be seen in Fig. 8, the best deformation found gives only a moderate improvement of the beam quality, even when combined with the optimised input coupling. Indeed, the best result comes from using the undeformed square waveguide with the optimised input coupling. It was not possible to translate the good improvement found in [6] for an ITER RSL to 140 GHz. While this result is disappointing, the investigations are still being pursued with other classes of deformations.

6 Fabrication

The 2 RSLs were fabricated at the industrial partners. In order to achieve vacuum tightness and high quality corrugations, a galvano-plastic (electroforming) technique was used. For each RSL, the 2 straight parts and the mitrebend were manufactured as one piece, respectively.

DOI: 10.1051/epjconf/201714704004

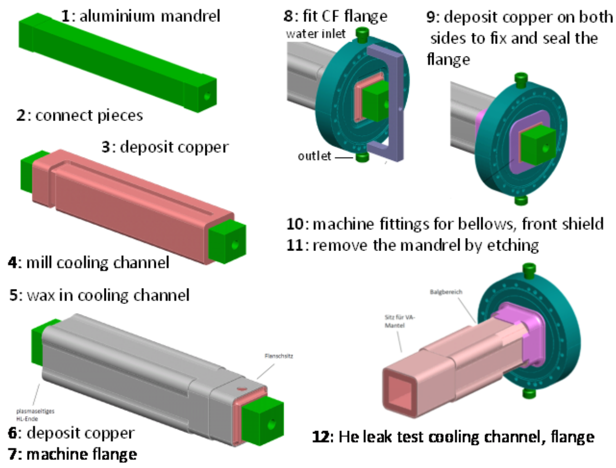

Figure 9. Electroforming fabrication process for the corrugated square waveguide (length is understated for illustration purposes.)

The negative form was machined in aluminium, and the copper material subsequently galvanised on top (see Fig. 9). Specialised milling tools were built to precisely and efficiently mill the corrugation grooves into the aluminium mandrel. Cooling channels were milled into the aluminium and closed by additional electroforming.

7 Results of low power tests

The finished RSL1 and RSL5 were transported to IGVP for low-power testing and beam characterisation. Fig. 10 shows the setup of RSL1 with the input mirror and diamond window. For each waveguide, the full setup with 2 straight pieces, the mitrebend, vacuum valve, diamond window, and coupling optics was set up. A vector network analyser was used as the source, with the receiving antenna mounted on a 2D movable platform at the output side.

The far field measurements (at a distance of 1 m) are shown in Fig. 11 for various steering angles. The output beam is clearly defined, and the side lobes are moderate. A similar result was obtained for RSL5.

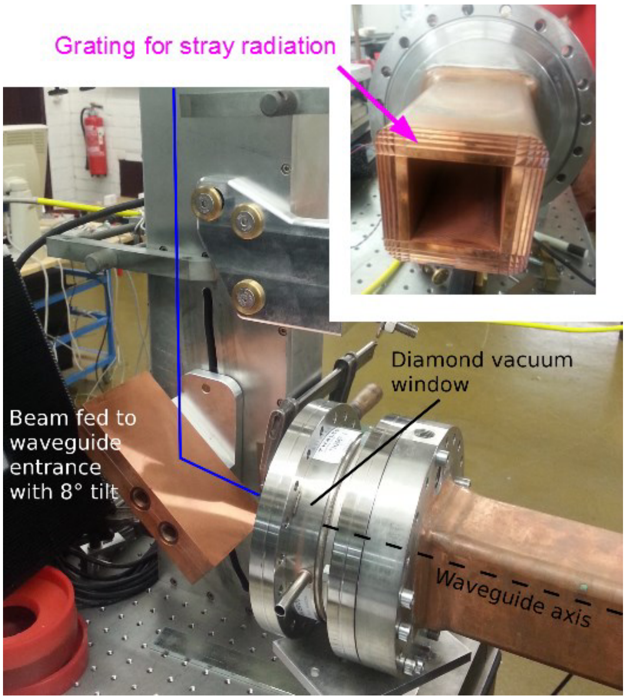

Figure 10. Input side of the finished RSL1 with optimised input coupling optics. The inset shows the other end of the straight waveguide piece.

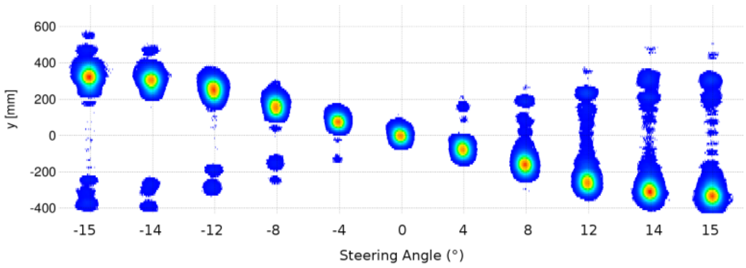

Figure 11. Far field measurements for RSL1. The steering effect is clearly seen and the side lobes are moderate (linear scale).

The output beam quality was assessed using near field measurements directly at the mouth of the waveguide. A fine spatial sampling was used to capture both the amplitude and the phase of the beam. A Gaussian beam was fitted to the data. The fraction of total power in this Gaussian beam was taken as the efficiency of the beam.

At 0°, a Gaussian with a waist size of 15.6 and 14.5 mm for E and H plane was found, respectively. The phase front was flat. For the optimised angle 12.7°, a phase front tilt of 12.6° was found, in very good agreement with the expected beam. At the optimised angle, it is expected that the beam is perfectly centred on the waveguide axis (no lateral shift necessary). However, a 5 mm shift was found. The shift only disappeared at 14.5°, which would hint that the waveguide was effectively shorter and its optimal steering angle therefore larger.

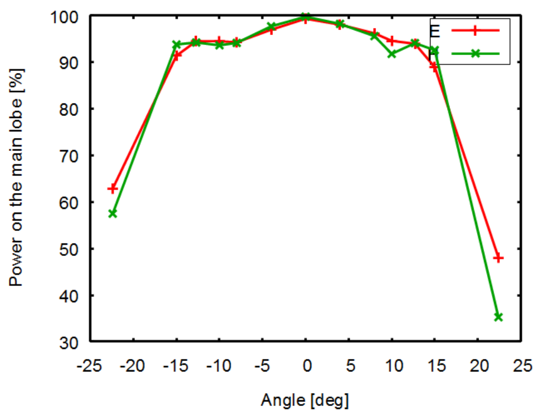

Figure 12. Beam quality measurements in the near field, E and H plane.

Nevertheless, the beam quality (shown in Fig. 12) was still very good for steering angles between -15˚ and 15˚. Only the revival beams (expected at 22.4˚) were unusable. Due to the effective shortness of the waveguide, their angles, too, would be shifted to larger values.

The explanation for this shortening of the waveguide can be found be examining the effective waveguide width a: For a square corrugation profile, the real and the effective groove depth are both λ/4, but for the rounded profile, the actual profile depth is slightly larger than that to have the same effect. If the wave then penetrates slightly into the grooves, the effective waveguide width increases, which means that the nominal length L also increases (see Eq. (2)). Since this was not taken into account, the waveguide is a few cm too short, which explains the observed behaviour.

The design of the optimised input coupling has been updated to take the new optimal angle into account.

8 Conclusions

The BMBF project FORMIK[3] was brought to a successful conclusion. The performance of the 2 RSLs was characterised with low power measurements and found to be good with moderate side lobes. They were delivered to W7-X, where they are awaiting installation and high power tests.

The design and manufacturing experience gained will be very valuable for DEMO where remote steering has to be considered because of the harsh reactor environment and the dearth of large ports.

Acknowledgements

This work is supported by the German Ministry of Education and Research (BMBF) by grant 03FUS0017A.

References

1. V. Erckmann et al., Electron cyclotron heating for W7-X: Physics and Technology. Fusion Science and Technology **52**, No 2 (2007) 291-312.
2. W.H.F. Talbot, Facts relating to optical sciences. No. IV. Philos. Mag. 9 (Third series), **401** (1836).
3. K. Ohkubo et al., “Extension of steering angle in a square corrugated waveguide antenna”. Fusion Eng. Des. **65** (2003), 657 – 672.
4. B. Plaum et al. “Numerical calculation of reflection characteristics of grooved surfaces”. J. Infrared Milli. Terahz. Waves **32** (2011), 482–495.
5. C. Lechte “Investigation of the Scattering Efficiency in Doppler Reflectometry by Two-Dimensional Full-Wave Simulations” IEEE Trans. Plas. Sci. **37** No 6, 2009, 1099-1104
6. G. G. Denisov et al: “Efficiency enhancement of components based on Talbot effect”. Int. J. Infrared Milli. Waves 28 (2007), 923–935